The International Journal of Advanced Manufacturing Technology (2024) 132:5305–5314
https://doi.org/10.1007/s00170-024-13674-w

ORIGINAL ARTICLE

The effect of weld heat input on the microstructure and mechanical properties of wire arc additively manufactured 15-5PH stainless steel

J Iain Sword[1] · Alexander Galloway[1] · Athanasios Toumpis[1]

Received: 27 December 2023 / Accepted: 19 April 2024 / Published online: 30 April 2024

Abstract

Precipitation hardening (PH) stainless steels, such as 15-5PH, have a high strength combined with excellent corrosion resistance. These properties make them valuable in critical industries such as defence, construction, aerospace, energy and maritime. Recent advancements in additive manufacturing (AM) technology enable the rapid and cost-effective production of components. In the case of 15-5PH components manufactured using wire arc additive manufacturing (WAAM), the as-deposited mechanical properties are not suitable at present for industrial applications. This paper explores the mechanical properties of this process and alloy combination without post weld heat treatment with the aim of eventual adoption in this condition by industry. The impact of weld heat input on the microstructure and mechanical properties of stainless steel 15-5PH produced using WAAM was investigated. The microstructure was examined using hardness testing in addition to optical and electron microscopy. Furthermore, mechanical properties were measured with tensile and impact testing. Investigations were conducted on material produced using weld heat inputs of 0.223 kJ/mm and 0.565 kJ/mm. These results indicate that reducing the weld heat input leads to a minor decrease in strength but an 80% increase in impact toughness. This reduction in weld heat input is correlated with a 50% reduction in volume fraction of δ-ferrite while also noting a 55% increase in carbide precipitates. In addition, the fracture surfaces were predominantly cleavage or quasi-cleavage in morphology.

Keywords Wire arc additive manufacturing · Metal additive manufacturing · Precipitation hardening stainless steel · Additive manufacturing process parameters · Mechanical testing

1 Introduction

Wire arc additive manufacturing (WAAM) is a modern manufacturing technique, using the principles of fusion welding to deposit material. This process uses an electrical arc to melt a feedstock wire, depositing a component of the desired shape. The capability of this process to reduce lead times [1] and material waste [2] is advantageous for the production of high value components in industries such as defence, construction, maritime, energy and aerospace [3–6]. These components are often manufactured from materials such as titanium alloys [7], nickel-based superalloys [8, 9] and precipitation hardening (PH) stainless steels [10]. In addition, this process can reduce the environmental impact of manufacturing such components [11].

Alloy 15-5PH is a martensitic, PH stainless steel [12] widely used in the aerospace, marine and energy industries for its high strength and corrosion resistance [13]. Many industries are investing in the transition from conventional manufacturing, such as machining or forging, to AM (additive manufacturing) technologies including WAAM. To make this change viable, a set of process parameters must be identified to achieve bulk mechanical properties equal to or superior to those achieved by conventional manufacturing [14]. The key factor in the processing of PH stainless steels is the thermal history during manufacturing, particularly when high temperatures are experienced by the material

Highlights
- WAAM of 15-5PH stinless steel is sensitive to changes in process parameters.
- Mechanical properties produced exceed those previously published in the as-deposited condition.
- Low weld heat input during deposition leads to enhanced impact toughness due to reduced δ-ferrite fraction.

✉ J Iain Sword
james.sword@strath.ac.uk

[1] Department of Mechanical & Aerospace Engineering, University of Strathclyde, James Weir Building, 75 Montrose Street, Glasgow G1 1XJ, UK

such as during welding, casting, forging or AM techniques [15, 16]. Control of mechanical properties for PH stainless steels can also be achieved through heat treatment, where the material is typically supplied in a solution treated condition [13] and an aging treatment is performed to develop precipitates which increase strength [17].

The development of corrosion resistant alloys such as PH stainless steels as feedstocks for the WAAM process is not yet extensively investigated [18]. The microstructure and tensile strength have been previously investigated for thin plates joined using gas tungsten arc welding (GTAW) [19] which reports low elongation and reduced strength when the as-welded material is compared to equivalent wrought material. A related study has investigated the mechanical properties of PH stainless steel plates requiring multi-pass welding [20] showing that quasi-cleavage fracture is expected and leads to strength levels far below those specified by ASTM A693 [12]. Early research into the use of PH stainless steels for the WAAM process has been performed using cold metal transfer (CMT) deposition [10]. This variant of gas metal arc welding (GMAW) advances and retracts the filler wire to deposit small droplets of liquid metal many times a second. This results in a reduced weld heat input compared to conventional GMAW deposition and improves control over the weld bead profile [21].

The results of Caballero et al. [10] and Guo et al. [22] investigate the mechanical properties of 17-4PH produced using CMT-WAAM. They demonstrated low strength in the as-deposited condition due to the retention of interdendritic δ-ferrite. This is a body centred cubic phase [23] found in many stainless steel alloys in varying quantities [24] and must be controlled during welding [25]. In stainless steels, δ-ferrite evolves during the solidification of the alloy, followed by austenite and martensite through diffusion and shear transformation [26]. Due to the rapid solidification found during the WAAM process, little austenite is retained, leading to significant levels of δ-ferrite [27]. An increase in the δ-ferrite fraction of these alloys has been correlated with a reduction in toughness in stainless steels [28, 29].

The primary strengthening constituents of 15-5PH include niobium carbides (NbC), copper precipitates [22] and additional metal carbides of compositions M_7C_3 and $M_{23}C_6$. $M_{23}C_6$ carbides are formed during aging and are rich in Cr [15]. Changes in both the path strategy and weld heat input result in differences in bead geometry, microstructure [30] and thermal history [31] leading to improved mechanical properties. It is proposed herein that optimising the process parameters will improve the strength of this material in the as-deposited condition. This can be achieved by minimising the evolution of δ-ferrite and increasing the evolution of strengthening phases such as carbides and copper precipitates.

A previous study by Niu et al. [20] has developed impact toughness data at −20 °C for multi-pass GTAW welds following a range of post weld aging heat treatments (580 °C, 600 °C, 620 °C for 4 h). This shows an increase in impact toughness as the aging temperature is increased. The impact toughness of 15-5PH has not yet been studied for material produced by WAAM.

The strength of 15-5PH produced by WAAM, as reported to date [10, 22], is notably lower than that specified for wrought material. However, by controlling the δ-ferrite evolution, the present work demonstrates an improvement in strength for this material and process combination. In addition, data is presented on the resulting impact toughness, which is valuable for the consideration of this material and process in future industrial applications.

2 Materials and methods

The bulk material produced for this work was a wall of deposited material of dimensions 235 mm × 30 mm × 110 mm manufactured using an additive manufacturing cell. This cell was composed of an ABB 2400 L robot arm controlled by an ABB IRC5 control cabinet and teach-pendant in addition to a Fronius CMT fusion welding torch, power supply and wire feed.

The shielding gas was high-purity argon and the substrate was EN32B low carbon mild steel. Commercially available 15-5PH welding wire of 1.2 mm diameter was used as a feedstock with the chemical composition of the feedstocks which is shown in Table 1 as provided in the suppliers datasheets.

Two sets of process parameters were tested to vary the weld heat input. These values are shown in Table 2 and subsequently referred to as HH and LH. The resulting parameters were obtained from settings within the robot

Table 1 Chemical composition of material feedstocks

Chemical element %	Material	Ni	Cr	Fe	Nb	Cu
Filler wire	15-5PH	4.89	14.5	Bal.	0.141	2.94
Substrate	EN32B	-	-	Bal.	-	-
Chemical element %	**Material**	**Mn**	**Si**	**C**	**P**	**S**
Filler wire	15-5PH	0.497	0.331	0.07	0.020	0.002
Substrate	EN32B	0.70	0.22	0.15	0.016	0.010

Table 2 Process parameters for WAAM production

Parameter	Travel speed (mm/s)	Wire feed speed (m/min)	Standoff distance (mm)	Interpass temperature (°C)
High weld heat input (HH)	4	6.5	15	200
Low weld heat input (LH)	10	6.5	15	200
Parameter	Current (A)	Voltage (V)	Weave	Energy input (kJ/mm)
High weld heat input (HH)	157	18.0	2 mm circular	0.565
Low weld heat input (LH)	173	16.1	n/a	0.223

and welding control systems and the interpass temperature measured with a digital thermometer probe. Weld heat input was calculated using Eq. 1 from BE EN 1011-1 [32]. In this equation, Q is the weld heat input, k is the thermal efficiency (0.8 for MIG welding), V and I are the voltage and current of the arc and v is the arc travel speed.

$$Q = k\frac{V \cdot I}{v} \cdot 10^{-3} \text{ in kJ/mm} \quad (1)$$

Samples were extracted from the bulk wall and prepared by standard metallographic grinding and polishing techniques followed by etching with Kalling's no. 2 reagent. Examination of the microstructure was performed using an Olympus GX51 inverted microscope. Microhardness measurements were taken on these same samples using a Q-Ness 60 A + automated hardness tester with a 0.05 kg load.

The point count method from ASTM E562-19 [33] was used to quantify the δ-ferrite volume fraction with 3 fields of 100 points on each of the HH and LH material and compared to the microstructural images from Guo et al. [22].

Tensile samples and Charpy impact samples were produced from the bulk material as indicated in Fig. 1. The tensile and impact testing samples were extracted from the bulk material by water-jet cutting before milling to shape. The dimensions of these samples were derived from standards ASTM-E8 [34] and BS EN ISO 148 [35], respectively. Tensile testing was performed using an Instron 8802 servo-hydraulic universal testing machine with a capacity of 250 kN in accordance with ASTM-E8. Charpy impact testing was performed using a Losenhausenwerk 14,590 Charpy impact apparatus with a capacity of 290 J at 20 °C.

3 Results and discussion

3.1 Microstructure

Figure 2 shows micrographs of the samples manufactured using both HH and LH parameters at mid-height of the deposition, being representative of the bulk microstructure in larger components. The resulting material is characterised by a dendritic microstructure with a martensitic matrix and interdendritic δ-ferrite (Fig. 2(i)). A directional columnar microstructure is noted due to solidification of dendrites in the direction of cooling (Fig. 2a) at low magnification.

Differences can be noted when comparing the microstructures which evolve with these different parameters. When analysed using the method presented in ASTM E562 [33], the material produced using high weld heat input (HH) displays a δ-ferrite fraction of 12%, while the material produced with a low weld heat input (LH) reduces the δ-ferrite fraction to 6.7%. When this method is applied to the micrographs provided in Guo et al. [22], a δ-ferrite fraction of 22% is found. The number of carbide precipitates in each

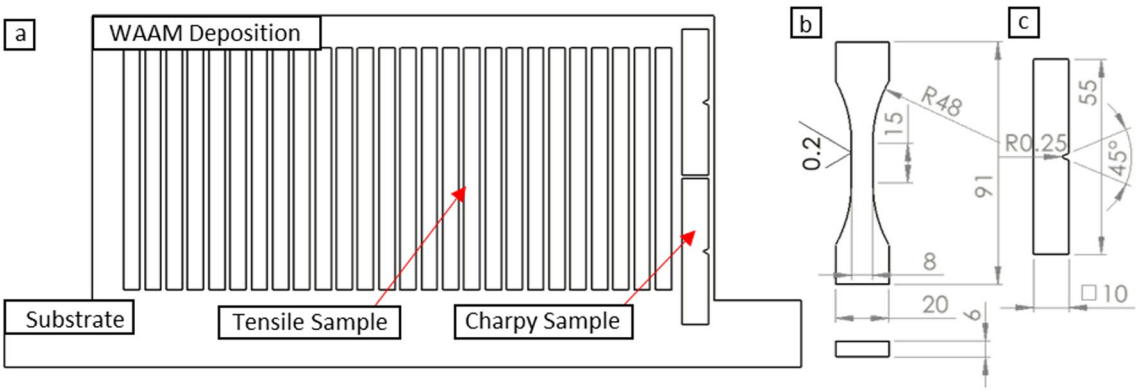

Fig. 1 Schematic of samples extracted from WAAM deposited material (**a**), dimensions of tensile sample (**b**) and Charpy sample (**c**)

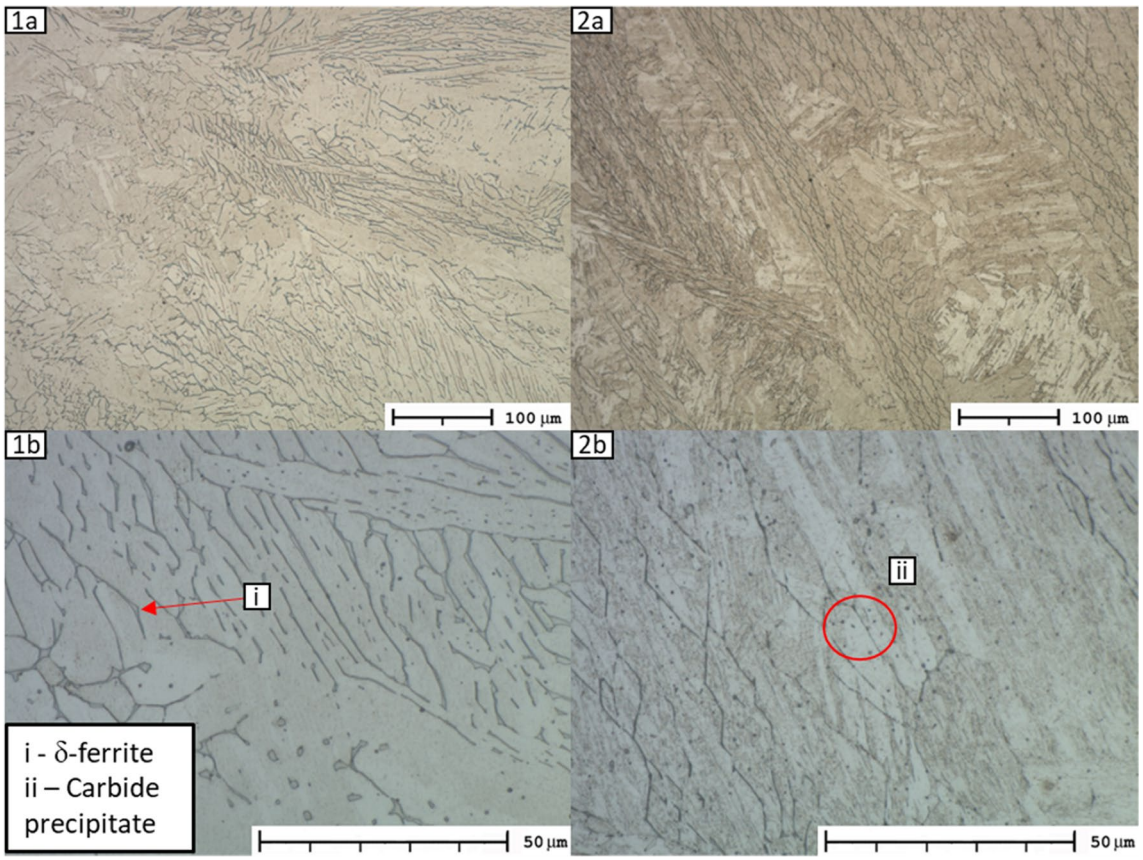

Fig. 2 Micrographs of WAAM-produced 15-5PH with high heat input during deposition (1a) and (1b) (HH) and low heat input during deposition (2a) and (2b) (LH)

micrograph (Fig. 2(ii)) was also totalled within equivalent areas. It is noted that the carbide count increases by 100% as the weld heat input is reduced. A comparison of these with 95% confidence intervals is shown in Fig. 3. An examination of these constituents under SEM and using an EDS sensor will allow the chemical composition to be determined, for example the locations indicated in Fig. 4. Locations (i) and (ii) were determined to have composition matching that of the alloy, with their morphology indicating martensite and δ-ferrite are present. The precipitates, such as location (iii), were identified to have a composition rich in carbon suggesting the presence of large carbides within the matrix. Copper precipitates and niobium carbides are expected within this alloy but were not identified due to their small size (3 and 300 nm, respectively) [16, 20]

3.2 Mechanical property testing

Figure 5 shows the results for Vickers microhardness testing with 250 indents. The results show greater hardness correlates with lower weld heat input during deposition (LH). When compared to the material standard A693 [12], it was found that the results for HH material closely correlated with the specified hardness of heat treatment H1025. It was also found that the LH material met the hardness requirements for H900.

Tensile testing displayed that the greater weld heat input deposition (HH) resulted in greater yield, UTS and elongation when compared to reduced weld heat input as shown in Fig. 6. In both conditions, all properties meet the requirements for material in the H1150 condition specified in A693 [12].

Finally, the impact testing results shown in Fig. 7 illustrate that low weld heat input (LH) resulted in a significantly higher impact toughness, meeting the requirements for H1025 and H1150, while the high weld heat input material (HH) did not meet any requirements for impact toughness specified by ASTM A693 [12].

3.3 Fractography

The fracture surfaces were examined to determine the failure modes and identify differences in the mechanism leading to failure between weld heat input conditions during deposition. The fracture surfaces produced during tensile

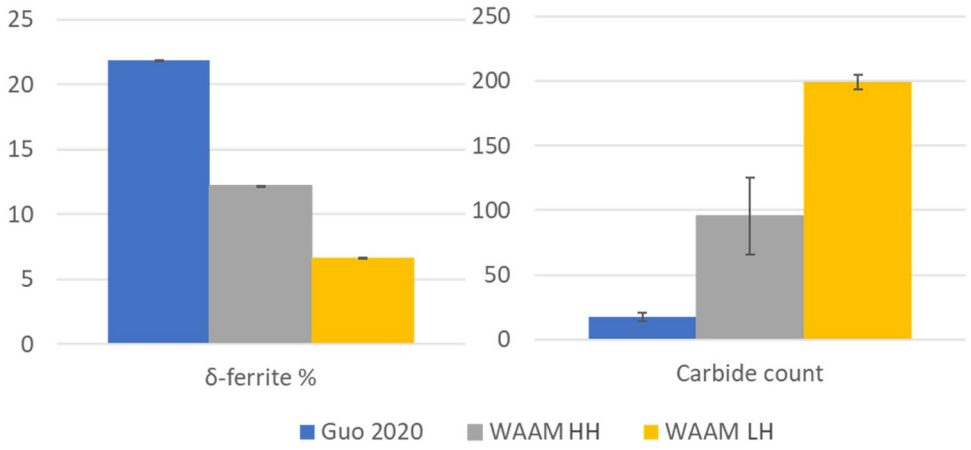

Fig. 3 δ-ferrite volume fraction % and carbide count comparison for WAAM-produced 15-5PH using high and low weld heat input during deposition compared with data from Guo et al. [22]

testing are shown in Fig. 8; they show that failure is dominated by cleavage in the HH material, while a combination of ductile rupture and quasi-cleavage is prominent in the LH material.

When the fracture surfaces of the samples tested for impact toughness are examined, a similar trend is noted in Fig. 9, with HH material showing cleavage features across the fracture surface. When LH material is considered, quasi-cleavage is only noted near the notch, with most of the fracture surface displaying dimple rupture with shear wings developing at the edges of the sample.

3.4 Discussion

The weld heat input during deposition is shown to have a significant impact on the mechanical properties of PH stainless steel. The as-deposited condition was compared against standard A693 [12] in addition to existing literature using the same process and material with variations in weld heat input. This comparison is shown in Table 3 with the HH material displaying superior mechanical properties to the results from both Caballero et al. [10] and Guo et al. [22].

When the LH material is considered, yield strength is shown to be superior to the existing literature while UTS and elongation are comparable to results previously presented. When compared against standard A693 [12], the results for LH material in the as-deposited condition meet the requirements for wrought 15-5PH in the H1150 condition for all properties except hardness. The latter is higher than specified due to a higher concentration of carbides compared to the wrought alloy.

An examination of the fracture surfaces indicates that the HH material experienced brittle fracture, while the dominant mode of failure for the LH material was ductile rupture during tensile testing. This corresponds with the results presented in Niu et al. [20] where post weld heat treatment results in ductile failure and an increase in impact toughness.

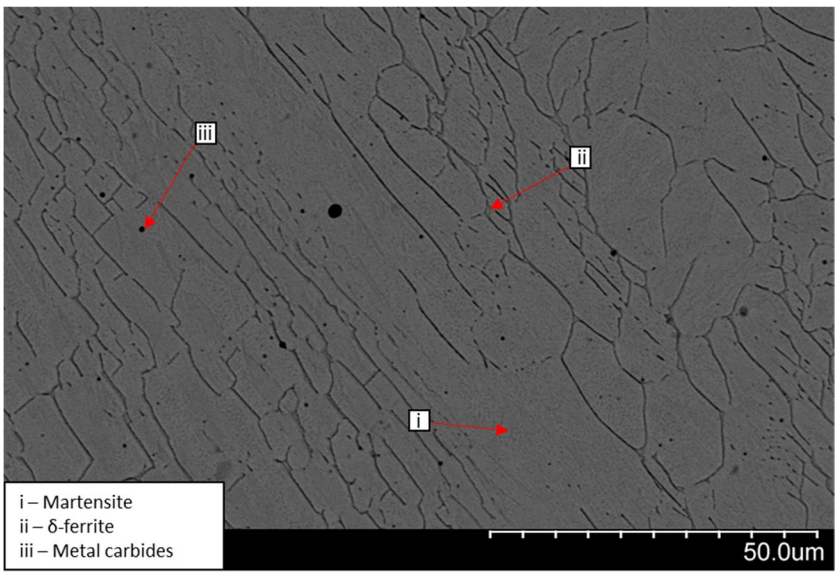

Fig. 4 SEM micrograph of WAAM-produced 15-5PH identifying the phases present

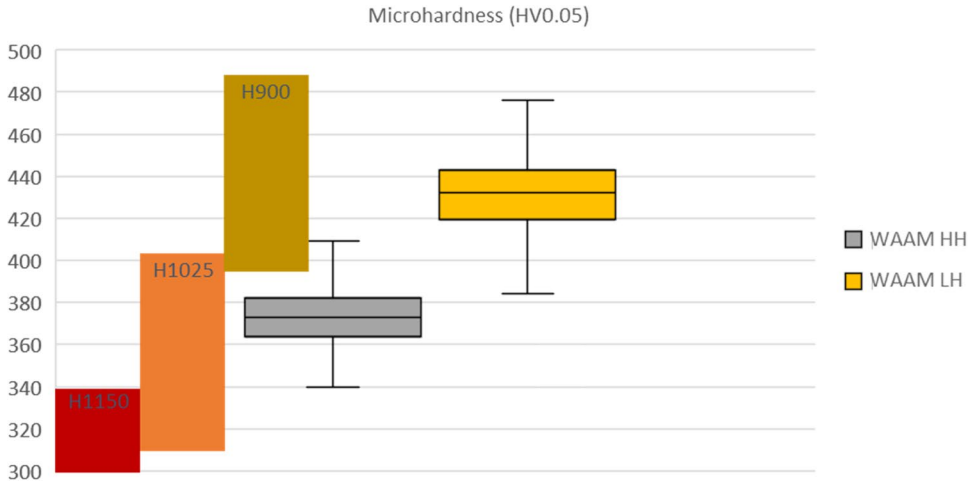

Fig. 5 Microhardness values from WAAM-produced 15-5PH using high and low weld heat input during deposition compared with values from A693 [12]

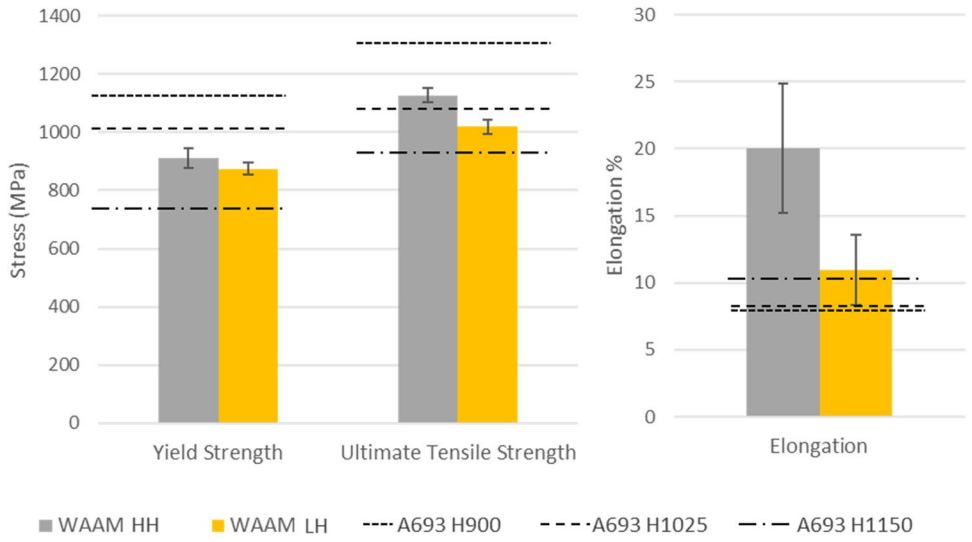

Fig. 6 Results from tensile testing of WAAM-produced 15-5PH using high and low weld heat input during deposition compared with values from A693 [12]

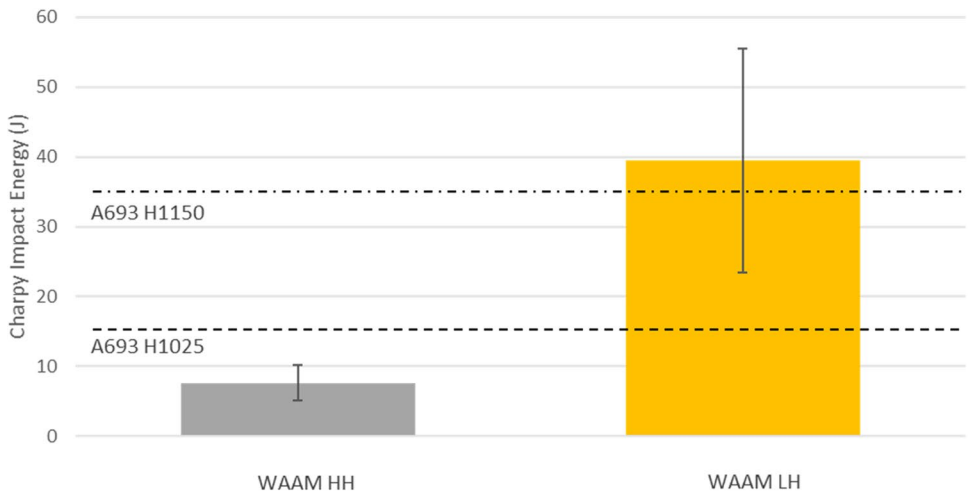

Fig. 7 Results from Charpy impact testing of WAAM-produced 15-5PH using high and low weld heat input during deposition compared with values from A693 [12]

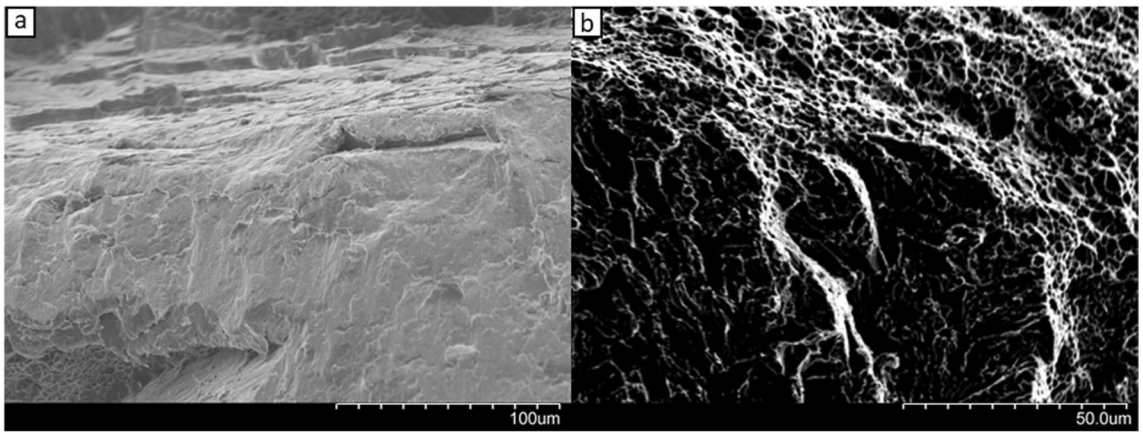

Fig. 8 SEM imaging of the fracture surfaces of tensile samples produced by HH (**a**) and LH parameters (**b**)

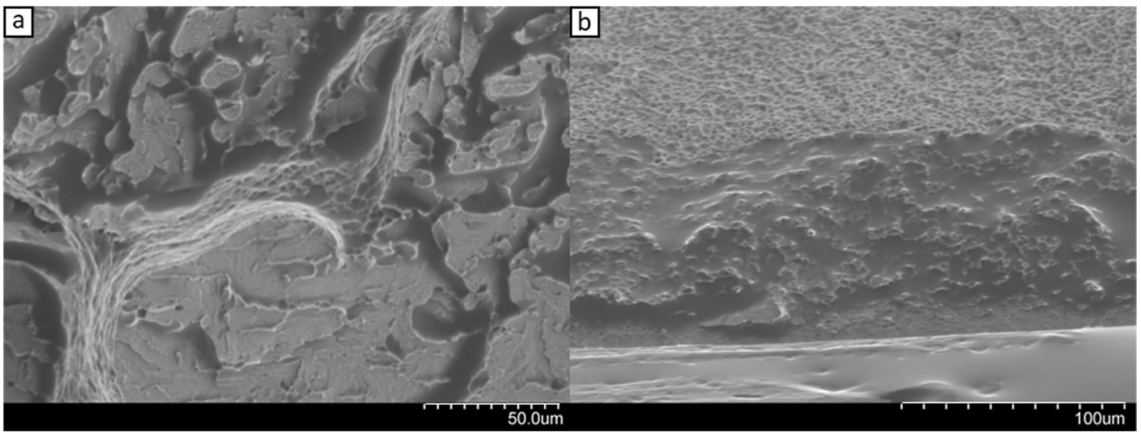

Fig. 9 SEM imaging of the fracture surfaces of Charpy impact samples produced by HH (**a**) and LH parameters (**b**)

Table 3 A comparison of testing results from WAAM-produced 15-5PH against material standard ASTM A693 [12]

Material condition	Yield strength (MPa)	Ultimate tensile strength (MPa)	Elongation %	Hardness (HV)	Charpy impact energy (J)	δ-ferrite fraction (%)
WAAM						
HH	910	1137	20.1	374	8	12.2
LH	875	1020	11.0	431	40	6.7
Caballero [10]	738	979	12.2	340	-	-
Guo [22]	666	1080	5.0	350	-	21.85
ASTM A693 [12]						
H900	1170	1310	8	388–490	n/a	-
H1025	1000	1070	8	311–406	14	-
H1150	725	930	10	258–342	34	-

There is an inconsistency between the elongation measured during tensile testing and the recorded impact toughness. In many metallic materials, increased elongation will also be associated with increased impact toughness [36]. However, this inconsistency has also been observed in other steel alloys containing δ-ferrite. For example, studies by Wang et al. [37] on stainless steel 13-4 and Rosenauer et al. [38] on 13-8PH noted a decrease in impact toughness when δ-ferrite concentration is increased, which corresponds with the results presented in Table 3.

The HH material displays a larger fraction of δ-ferrite which leads to the embrittlement of the WAAM deposited material [39]. The reduced weld heat input in LH material results in a reduction in the δ-ferrite fraction and improved impact toughness, while the prevalence of carbides within this material corresponds with the increase in hardness over the HH material. It is proposed that δ-ferrite present within WAAM deposited 15-5PH alloy leads to a decrease in hardness, resulting in differences in the microstructure and mechanical properties.

The alloy 15-5PH is frequently used in the manufacture of aerospace components such as landing gear, actuators and fasteners. These applications require a high corrosion resistance [40] and high strength to resist the stresses and harsh environment of aerospace service [17]. In addition, such components must be designed to reduce weight, taking advantage of "design for additive manufacturing" techniques. Therefore, the material must respond well to additive manufacturing processes to produce components with suitable properties [1, 41, 42]. As such, the LH process parameters are recommended, due to their reduced δ-ferrite volume fraction, improving corrosion resistance in addition to high impact toughness and relatively high strength.

4 Conclusions

In this study, the impact of weld heat input on the microstructure and mechanical properties of as-deposited 15-5PH stainless steel manufactured through WAAM was investigated. The conclusions can be summarised as follows.

- The process parameters presented in this study demonstrate the higher mechanical properties than previously published in the literature for this material and process. The low weld heat input (LH) parameters meet the requirements for all mechanical properties except hardness for wrought alloy in the H1150 condition in ASTM A693. The excess hardness is attributed to an increase in carbides within the microstructure.
- Increased weld heat input (HH) results in an increased δ-ferrite volume fraction within the microstructure due to a reduction in the cooling rate during the WAAM process. This results in lower impact toughness compared to LH material, which displays a lower δ-ferrite volume fraction and a corresponding higher impact toughness and hardness.
- The difference in microstructure between HH and LH results in changes in the fracture behaviour in both impact and tensile testing, with HH samples exhibiting brittle fracture, while LH samples display evidence of ductile rupture. Again, this is a consequence of the variation in δ-ferrite volume fraction.
- An inconsistency has been observed between the elongation and impact results; this difference can be attributed to the variation in volume fraction of δ-ferrite. In this WAAM-produced material, it is noted that the increased δ-ferrite fraction in HH leads to an increase in elongation, but a reduction in impact toughness, making the LH condition more favourable.

Acknowledgements The authors would like to thank Glenalmond Technology for the provision of the additive manufacturing cell with which the bulk material was produced.

Author contribution All authors contributed to the study conception and design. Material preparation, data collection, and analysis were performed by J. Iain Sword. The first draft of the manuscript was written by J. Iain Sword, and all authors commented on previous versions of the manuscript. All authors read and approved the final manuscript.

Declarations

Conflict of interest The author declares no competing interests.

References

1. Atzeni E, Salmi A (2012) Economics of additive manufacturing for end-usable metal parts. Int J Adv Manuf Technol 62:1147–1155. https://doi.org/10.1007/s00170-011-3878-1
2. Martina F, Williams S (2015) Wire + arc additive manufacturing vs. traditional machining from solid a cost comparison. Cranfield University
3. Busachi A et al (2017) A review of additive manufacturing technology and cost estimation techniques for the defence sector. CIRP J Manufact Sci Technol 19:117–128. https://doi.org/10.1016/j.cirpj.2017.07.001

4. Wu W (2014) Additive manufacturing in offshore & marine - a materials perspective, <https://www.researchgate.net/publication/324834087_Additive_Manufacturing_in_Offshore_Marine_-_A_Materials_Perspective. Accessed 5/10/2020
5. Chandrasekaran S, Hari S, Amirthalingam M (2020) Wire arc additive manufacturing of functionally graded material for marine risers. Materials science & engineering. A, structural materials: properties. Microstruct Process 792:139530. https://doi.org/10.1016/j.msea.2020.139530
6. Evans SI et al (2022) A review of WAAM for steel construction – manufacturing, material and geometric properties, design, and future directions. Struct (Oxford) 44:1506–1522. https://doi.org/10.1016/j.istruc.2022.08.084
7. Lin Z, Song K, Yu X (2021) A review on wire and arc additive manufacturing of titanium alloy. J Manuf Process 70:24–45. https://doi.org/10.1016/j.jmapro.2021.08.018
8. Graybill B et al (2018) Additive manufacturing of nickel-based superalloys. ASME 2018 13th International Manufacturing Science and Engineering Conference - Volume 1: Additive Manufacturing; Bio and Sustainable Manufacturing. https://doi.org/10.1115/MSEC2018-6666
9. Kalyankar V, Bhoskar A (2021) Influence of torch oscillation on the microstructure of Colmonoy 6 overlay deposition on SS304 substrate with PTA welding process. Metall Res Technol 118:406. https://doi.org/10.1051/metal/2021045
10. Caballero A et al (2019) Wire + arc additive manufacture of 17 – 4 PH stainless steel: effect of different processing conditions on microstructure, hardness, and tensile strength. J Mater Process Technol 268:54–62. https://doi.org/10.1016/j.jmatprotec.2019.01.007
11. Sword JI, Galloway A, Toumpis A (2023) An environmental impact comparison between wire + arc additive manufacture and forging for the production of a titanium component. Sustainable Mater Technol 36:e00600. https://doi.org/10.1016/j.susmat.2023.e00600
12. ASTM-A693 (2016) A693-16 Standard specification for precipitation-hardening stainless and heat-resisting steel plate, sheet, and strip ASTM
13. Abdelshehid M et al (2007) On the correlation between fracture toughness and precipitation hardening heat treatments in 15-5PH stainless steel. Eng Fail Anal 14:626–631. https://doi.org/10.1016/j.engfailanal.2006.03.001
14. Wang Y, Xizhang C, Chuanchu S (2019) Microstructure and mechanical properties of Inconel 625 fabricated by wire-arc additive manufacturing. Surf Coat Technol 374:116–123. https://doi.org/10.1016/j.surfcoat.2019.05.079
15. Habibi Bajguirani HR (2002) The effect of ageing upon the microstructure and mechanical properties of type 15 – 5 PH stainless steel. Materials science & engineering. A, structural materials: properties. Microstruct Process 338:142–159. https://doi.org/10.1016/S0921-5093(02)00062-X
16. Couturier L et al (2016) Evolution of the microstructure of a 15-5PH martensitic stainless steel during precipitation hardening heat treatment. Mater Design 107:416–425. https://doi.org/10.1016/j.matdes.2016.06.068
17. Peng X-y et al (2015) Effect of aging on hardening behavior of 15 – 5 PH stainless steel. J Iron Steel Res Int 22:607–614. https://doi.org/10.1016/S1006-706X(15)30047-9
18. Asala G et al (2017) Microstructural analyses of ATI 718Plus® produced by wire-ARC additive manufacturing process. Metall Mat Trans A 48:4211–4228. https://doi.org/10.1007/s11661-017-4162-2
19. Prabhakar AS et al (2015) Effect of post weld heat treatment on mechanical properties of 17-4-PH stainless steel welds. Mater Sci Forum 830:181–184. https://doi.org/10.4028/www.scientific.net/MSF.830-831.181
20. Niu J et al (2020) Effect of Post-weld Aging temperature on microstructure and Mechanical properties of Weld Metal of 15 – 5 PH Stainless Steel. J Mater Eng Perform 29:7026–7033. https://doi.org/10.1007/s11665-020-05193-y
21. González J et al (2017) Additive manufacturing with GMAW welding and CMT technology. Procedia Manuf 13:840–847. https://doi.org/10.1016/j.promfg.2017.09.189
22. Guo C, Hu R, Chen F (2020) Microstructure and performances for 15 – 5 PH stainless steel fabricated through the wire-arc additive manufacturing technology. Mater Technol 1–12. https://doi.org/10.1080/10667857.2020.1800296
23. Zhang B et al (2022) Microstructure and mechanical properties of high-efficiency laser-directed energy deposited 15-5PH stainless steel. Mater Charact 190:112080. https://doi.org/10.1016/j.matchar.2022.112080
24. Barnard P (2017) 4 - Austenitic steel grades for boilers in ultra-supercritical power plants. In: (ed) Elsevier Ltd, pp 99–119
25. BSI (2018) BS EN ISO 8249:2018: welding. Determination of Ferrite Number (FN) in austenitic and duplex ferritic-austenitic Cr-Ni stainless steel Weld metals. British Standards Institute
26. Ghaffari M, Nemani AV, Nasiri A (2022) Microstructure and mechanical behavior of PH 13–8Mo martensitic stainless steel fabricated by wire arc additive manufacturing. Additive Manuf 49:102374. https://doi.org/10.1016/j.addma.2021.102374
27. García-García V et al (2022) Mechanical behavior of austenitic stainless-steel welds with variable content of δ-ferrite in the heat-affected zone. Eng Fail Anal 140:106618. https://doi.org/10.1016/j.engfailanal.2022.106618
28. Pant B et al (2012) Correlation of mechanical properties with Ferrite Number in 0.07 C-16Cr-6Ni stainless steel. Materials Science Forum 710:495–499. https://doi.org/10.4028/www.scientific.net/MSF.710.495
29. Hosseini A V et al (2019) Ferrite content measurement in super duplex stainless steel welds. Weld World 63:551–563. https://doi.org/10.1007/s40194-018-00681-1
30. Dinovitzer M et al (2019) Effect of wire and arc additive manufacturing (WAAM) process parameters on bead geometry and microstructure. Additive Manuf 26:138–146. https://doi.org/10.1016/j.addma.2018.12.013
31. Xu X et al (2019) Preliminary Investigation of Building Strategies of Maraging Steel Bulk Material using wire + Arc Additive manufacture. J Mater Eng Perform 28:594–600. https://doi.org/10.1007/s11665-018-3521-5
32. BS1011-1 (2009) BS EN 1011-1:2009: Welding. Recommendations for welding of metallic materials. General guidance for arc welding British Standards Institute
33. ASTM (2019) E562-19 standard test method for determining volume fraction by systematic manual point count
34. ASTM-E8 (2021) E8-21 standard test methods for tension testing of metallic materials ASTM
35. BS148-1 (2016) BS EN ISO 148-1:2016: metallic materials. Charpy pendulum impact test. Test method British Standards Institute
36. Coppard R et al (2019) Impact of carbon macrosegregation on the mechanical properties of low-alloy steel forgings. ASME 2019 Pressure Vessels & Piping Conference: Volume 6B: Materials and Fabrication. https://doi.org/10.1115/PVP2019-94059
37. Wang P et al (2010) Effect of delta ferrite on impact properties of low carbon 13Cr–4Ni martensitic stainless steel. Materials science & engineering. A, structural materials: properties. Microstruct Process 527:3210–3216. https://doi.org/10.1016/j.msea.2010.01.085
38. Rosenauer A et al (2022) Influence of delta ferrite on the impact toughness of a PH 13 – 8 Mo maraging steel. Mater Sci Eng A 856:144024. https://doi.org/10.1016/j.msea.2022.144024
39. Shiao JJ et al (1994) Aging embrittlement and lattice image analysis in a Fe-Cr-Ni duplex stainless steel aged at 400 deg C. J Nucl Mater 217:269–278. https://doi.org/10.1016/0022-3115(94)90376-X

40. Lara-Banda M et al (2020) Alternative to nitric acid passivation of 15 – 5 and 17-4ph stainless steel using electrochemical techniques. Materials 13:1–14. https://doi.org/10.3390/ma13122836
41. Lockett H et al (2017) Design for Wire + Arc Additive manufacture: design rules and build orientation selection. J Eng Des 28:568–598. https://doi.org/10.1080/09544828.2017.1365826
42. Wang Z, Zhang Y, Bernard A (2021) A constructive solid geometry-based generative design method for additive manufacturing. Additive Manuf 41:101952. https://doi.org/10.1016/j.addma.2021.101952